Irreversible Demagnetization Analysis for Multilayer Magnets of Permanent Magnet-Assisted Synchronous Reluctance Machines Considering Current Phase Angle

Thanh Anh Huynh and Min-Fu Hsieh

Department of Electrical Engineering, National Cheng Kung University, Tainan 701, Taiwan

This paper investigates the demagnetization problem of permanent magnets for permanent magnet-assisted synchronous reluctance motors (PMa-SynRM) and applies "demagnetization ratio" as an index to evaluate demagnetization of permanent magnet (PM). The PMa-SynRM is often designed with multilayer flux barriers to improve saliency and reluctance torque in the rotor. Weaker or less PM (than that for interior PM motors) is embedded into the rotor which could be demagnetized in high-performance operation. PM demagnetization involves temperature, current magnitude, current phase angle, designed PM operating point, or combined effect of the above factors. This work investigates the demagnetization risk for PMs in all the layers of PMa-SynRM rotor considering these factors. In particular, the current phase angle for flux weakening operation is often omitted in demagnetization analysis. First, the motor performance to satisfy the operation condition over a wide speed range is analyzed and the proportion of motor torque components, i.e., reluctance torque and electromagnetic torque, considering temperature is investigated. Then, the flux density distributions on PMs at each position/layer are studied and the PM operating points are obtained based on the variation of excitation current, current phase angle, and temperature in order to evaluate the demagnetization risk. The analysis suggests that the high current phase angle combining the effect of high temperature is the major cause of irreversible demagnetization. Finally, a method incorporating the index "demagnetization ratio" is proposed to redesign the PMa-SynRM to avoid demagnetization. Experiments are conducted to validate the simulation.

Index Terms— **Demagnetization ratio, magnet temperature, multilayer magnets, operating point, Permanent magnet-assisted synchronous reluctance motors (PMa-SynRM).**

I. Introduction

ELECTRIC vehicles (EVs) have been considered as a key technology for the automotive industry and transportation sector due to their low emission and environmental friendliness [1]. In EVs, the traction motors are the core component of propulsion systems and selecting a suitable traction motor is critical for EV performance.

Permanent magnet-assisted synchronous reluctance motors (PMa-SynRMs) are known as a potential candidate for traction motors for their decent torque density with low permanent magnet (PM) cost, high efficiency, and wide speed range [2]. The PMa-SynRM is often designed with weaker or less PM than that for an interior PM (IPM) motor. Therefore, demagnetization in high-performance operation (e.g., high armature current or flux weakening) is possible [3]. PM demagnetization may be caused by poor operating points, high armature current, rotor configurations, and deep flux weakening combining temperature effect [4]. The operating point of PMs in PMa-SynRM rotor can be different at each PM position/layer and their demagnetization risk is also different [3], [5]. However, the effect of the current phase angle, much needed for flux weakening operation, as well as its combined effect with the above factors, has not been fully studied.

Previous studies mainly focused on demagnetization due to the current magnitude and temperature [6], [7]. However, for EV traction motors, the speed range is broad and flux weakening is often required. This indicates that the high current phase angle would be employed for deep flux weakening. Based on this point, this paper considers the effect of the current phase angle since the q-axis current would impact on the PMs that are arranged facing the q-axis in PMa-SynRM rotors. Temperature rise would then increase the possibility of demagnetization.

This paper comprehensively investigates and evaluates the demagnetization risk at the PMs in all the layers of the PMa-SynRM rotor considering maximum current, temperature, and most importantly, the current phase angle. The temperature distribution across one PM piece is possibly different and this indicates that parts of the PM pieces can be more easily demagnetized than any other [8]–[11]. Meanwhile, the current magnitude and phase angle can vary the operating point of the PMs at different PMs in the rotor. For evaluation of possible demagnetization in the PM, the operating conditions of the PMa-SynRM over a wide speed range are first considered and the effect of motor temperature to the proportions of PM torque and reluctance torque in the total torque is investigated. Then, the PM flux density at each position/layer and the operating points of PMs are evaluated under the variation of excitation current, current phase angle, and temperature. From the analysis, the demagnetization ratio of PM at each position/layer in the PMa-SynRM is compared and discussed. Finally, a redesign process based on the index "demagnetization ratio" to calculate the new PM sizes for the PMa-SynRM is conducted so that PM demagnetization can be avoided. Simulations are conducted using JMAG. Experimental studies are carried out to validate the simulations.

Manuscript received November 6, 2018; revised February 28, 2019; accepted April 8, 2019. Date of publication May 16, 2019; date of current version June 20, 2019. Corresponding author: M.-F. Hsieh (e-mail: mfhsieh@mail.ncku.edu.tw).

Color versions of one or more of the figures in this paper are available online at http://ieeexplore.ieee.org.

Digital Object Identifier 10.1109/TMAG.2019.2911867

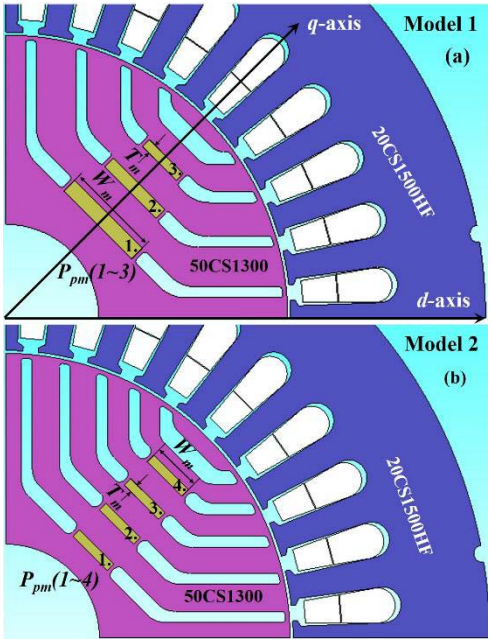

Fig. 1. Models of 10 kW PMa-SynRM, with magnet position and dq-axis indicated. (a) Model 1: different PM sizes. (b) Model 2: same PM size. Note that d-axis is the reference for the current phase angle.

TABLE I
MAIN SPECIFICATIONS AND PARAMETERS OF PMA-SYNRM

Parameters/Specs.	Model 1	Model 2
Peak power	10 kW	10 kW
Peak torque	67 Nm	67 Nm
Number of phase	3	3
Number of slots	36	36
Number of poles	4	4
Stator diameter	160 mm	160 mm
Rotor diameter	94 mm	94 mm
Stack length	120 mm	120 mm
Air-gap length	0.5 mm	0.5 mm
PM size	2.5x16, 2x12, 1.5x8 mm	1.5x8 mm
Stator/rotor Materials	20CS1500HF/50CS1300 (China Steel Corp.)	
Material of PM	N35H (NdFeB, B_r=1.21T at 20^{0}C, H_c=908 kA/m)	

Note that the "demagnetization ratio" may be used to evaluate demagnetization of PMs but this paper further incorporates this index into a design process proposed here that can avoid demagnetization.

II. INVESTIGATED MOTOR

A. Target Machine and Analysis Method

Two 10 kW PMa-SynRMs are designed and studied here with four and five flux barriers per pole and the PMs are added into three or four of them (except the outermost one), as shown in Fig. 1(a) and (b), respectively. The main specifications and materials for the motors are given in Table I. The PM utilized for both models is neodymium iron boron (NdFeB). The laminations used are 20CS1500HF for the stators and 50CS1300 for the rotors (both are products of China Steel Corporation, Taiwan), which have been previously mentioned in [3] and [5]. The PM positions in the two rotors are numbered in Fig. 1 and the dimensions of these PMs are given in Table I. The PM configurations for Models 1 and 2 are based on the PMa-SynRM models presented in [2], [3], and [5] with different research topics to this paper. As can be seen in Fig. 1 and Table I, the PM sizes of Model 1 decrease from position 1 to 3, whereas that for Model 2 is the same for all the positions. The dimensions for the outmost PMs of the two models are intentionally kept the same so that the demagnetization endurance for the two rotors can be compared. By these arrangements, the smallest PM size at position 3 for Model 1 or at position 4 for Model 2 may be vulnerable to demagnetization compared to PMs at other positions. In contrast, the arrangement with the same PM size in Model 2 allows an easy observation on position effect on demagnetization. The ability to resist demagnetization is also compared for the two models. It should be noted that the PM aspect ratio (defined as width to be divided by thickness) varies from 5.33 to 6.4. The difference is not significant. Finite-element analysis (FEA) is utilized to evaluate the demagnetization for the PMa-SynRM.

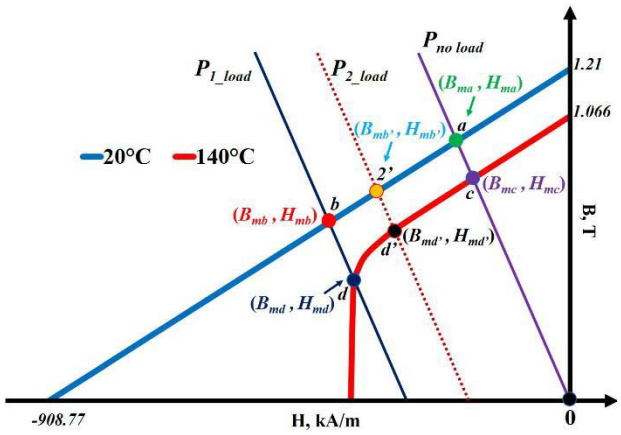

Fig. 2. Operating points of the PM with increasing temperature at no-load and load condition.

EV traction motors usually employ conductors with electrical insulation class B or higher (class F or H), depending on vehicle performance [12]. Thus, an operating temperature beyond 130 °C can possibly occur in some operating conditions, particularly for long-term operations. This increases the possibility of PM being demagnetized. This paper investigates the demagnetization risk of PM beyond 130 °C, which has been utilized to evaluate the demagnetization of PM motors in EV-related studies [11], [13].

B. Demagnetization Characteristics

Fig. 2 shows the demagnetization curves of Sintered NdFeB (N35H) whose maximum operating temperature is 140 °C [14]. Points a, b, and b', as indicated in Fig. 2, are the operating points of the PM under no-load (point a) and load conditions (points b and b') at 20 °C. Meanwhile, points c, d, and d' are the operating points at 140 °C under no-load (point c) and load conditions (points d and d'). Demagnetization can occur when the operating points of the PM are pushed low by the excitation current in load condition combining high temperature (e.g., line $P_{1-\text{load}}$ and point d). Therefore, the temperature and load conditions of

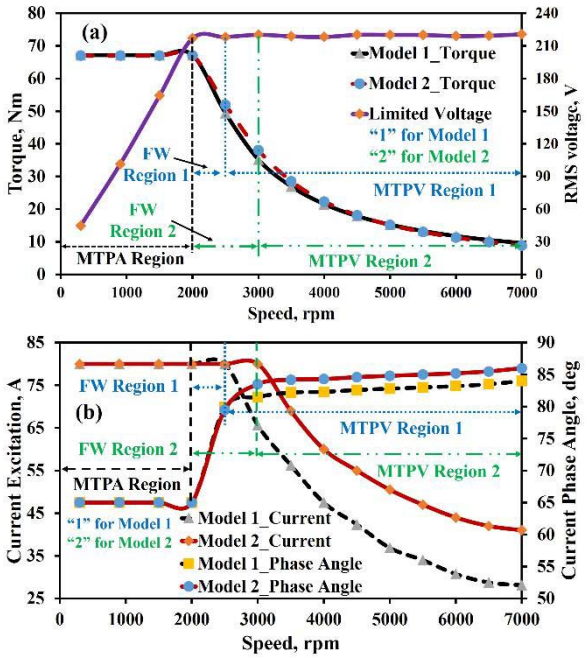

Fig. 3. Operation characteristics of PMa-SynRMs over the wide speed range. (a) Torque and voltage versus speed curves. (b) Current and phase angle versus speed curves.

the motor should be considered in the initial design to avoid demagnetization (e.g., line $P_{2-\text{load}}$).

As previously mentioned, the demagnetization risk of PM can be different in multilayer magnets of the PMa-SynRM. This indicates that the ratio of the "lost" magnetic flux density under load condition at each PM layer can be different. This index can be defined by "demagnetization ratio" and expressed as [15]

$$\text{Demagnetization Ratio} = \left(1 - \frac{B_{m2}}{B_{m1}}\right) 100\% \qquad (1)$$

where B_{m1} is the magnitude of the PM flux density for the case with temperature (20 °C) and B_{m2} is the magnitude of the PM flux density of a specified temperature.

Some studies [16], [17] have employed the demagnetization ratio for evaluation of demagnetization of PMs in motors; however, the motor operating conditions were not considered. In this paper, the calculated demagnetization ratio of PMs is not only utilized to evaluate demagnetization but also applied to a method proposed here for determination of PM size so that the demagnetization of PMa-SynRMs can be avoided when operating over a wide speed range with high temperature.

III. Motor Performance and Effect of Temperature to Torque Proportion

A. Motor Performance Over Wide Speed Range

The general requirements for EV traction motors are high torque/power density and high efficiency over a wide speed range. Therefore, the torque/power-speed characteristics of the PMa-SynRM are first studied. Fig. 3 shows the simulated torque-speed characteristic of the two PMa-SynRMs under the 220 V_{rms} input voltage limit and 80 A maximum current

TABLE II
Operation Characteristics of PMa-SynRM in Wide Speed Range

Items	MTPA	FW	MTPV
Model 1			
Speed	0-2000 rpm	2000-2500 rpm	2500-7000 rpm
Voltage Limit	0-220 Vrms	220 Vrms	220 Vrms
Induced Voltage	182.7V @ 2000 rpm	185.8V @ 2500 rpm	213.7V @ 7000 rpm
Input Current	80 A	80 A	80 - 28.1 A
Phase angle	65^0E	65^0 - 79.9^0 E	79.9^0 - 84^0 E
Model 2			
Speed	0-2000 rpm	2000-3000 rpm	3000-7000 rpm
Voltage Limit	0 - 220 Vrms	220 Vrms	220 Vrms
Induced Voltage	181V @ 2000 rpm	186V @ 3000 rpm	211V @ 7000 rpm
Input Current	80 A	80 A	80 - 41 A
Phase angle	65^0E	65^0 - 79.5^0 E	79.5^0 - 86^0 E

without considering temperature. As can be seen, within the speed range, the two PMa-SynRMs are operated in three regions: the maximum torque per ampere (MTPA) operation region, the field-weakening (FW) region, and the maximum torque per voltage (MTPV) operation region. The maximum torque of the two motors in the MTPA region is limited by the maximum current (80 A) under the 2000 rpm base speed. The operation in the FW region is to maintain the constant power over the speed range under the limitation of the input voltage and current excitation. For the MTPV region, the maximum speed can be achieved where the input voltage is limited by the maximum voltage and the input current is lower than the maximum current.

As can be seen in Fig. 3(a), the operation ranges for the FW and MTPV regions are 2000–2500 rpm and 2500–7000 rpm, respectively, for Model 1. For Model 2, they are 2000–3000 rpm for the FW region and 3000–7000 rpm for the MTPV region. The two motors may have different excitation currents and current phase angles although the torque-speed curves for them are almost the same. The operation characteristics of the two PMa-SynRMs in the three regions are summarized and shown in Table II, where the input current, current phase angle, and induced voltage are presented. Note that the related theory regarding PMa-SynRMs such as the voltage and torque equations can be referred to the literature [2], [3], [5] and will be repeated here to save space.

Based on the operating principles of PMa-SynRMs [5], the back magnetomotive force (MMF) should be reduced to increase the motor speed over the base speed. This is often conducted by manipulation of stator currents to weaken the flux. This leads to potential demagnetization of PMs for the PMa-SynRM, especially in the FW region when the temperature of the motor increases to a level. Moreover, the increase of temperature in the PMa-SynRM also reduces motor performance such as torque, power, and efficiency, which would be investigated in Section III-B.

B. Torque Proportion of Motor Under Temperature Effect

The operating characteristics of the two PMa-SynRMs at no-load and load conditions are first evaluated. Fig. 4(a) shows

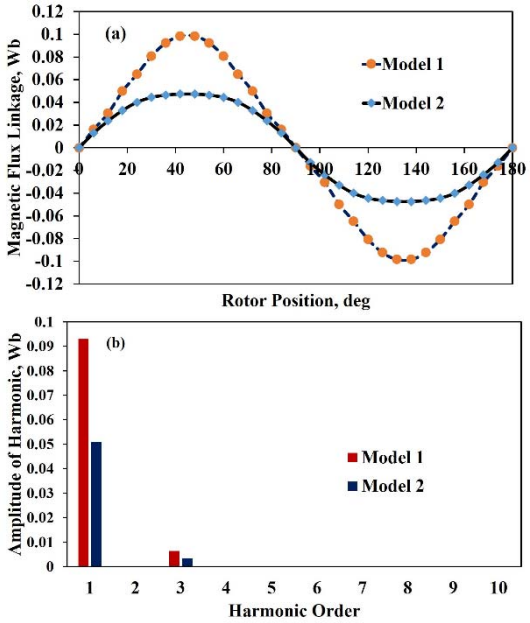

Fig. 4. Flux linkage and harmonic components of Phase A in PMa-SynRMs at no-load condition. (a) Magnetic flux linkage. (b) Harmonic amplitude.

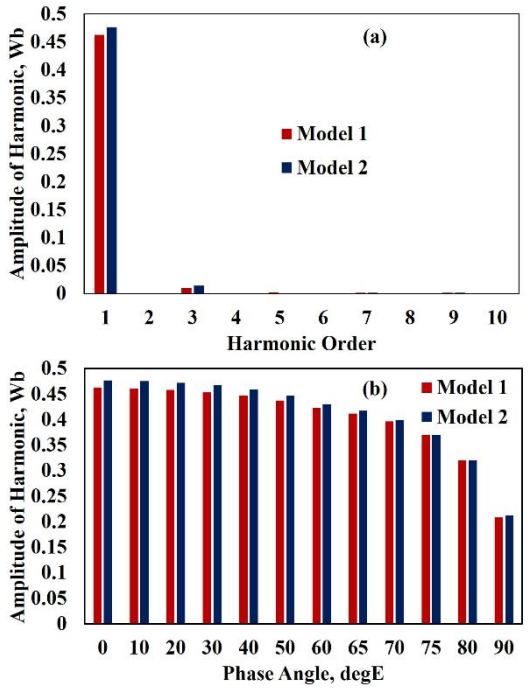

Fig. 5. Fundamental harmonic component of Phase A flux linkage for PMa-SynRMs at the load condition. (a) Magnitude is 0°E current phase. (b) Fundamental harmonic magnitude with the phase angle.

the flux linkage of the two models due to PMs at no-load condition, where Model 1 has a much higher magnitude than that of Model 2 because of its higher PM volume. Note that both models possess the same winding configuration. However, the flux linkage of Model 2 at the maximum current (80 A) is higher than that of Model 1, as shown in Fig. 5(a), where it is obtained when the current is applied on the d-axis. Then in Fig. 5(b), the current phase angle is advanced from the d-axis to the q-axis, and the magnitude of

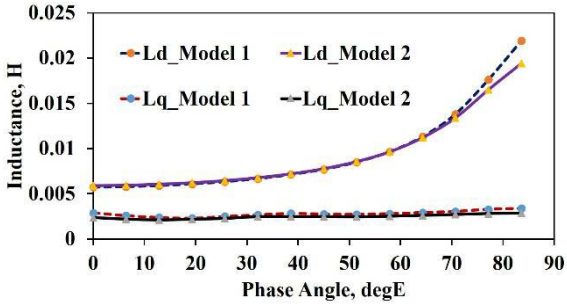

Fig. 6. Variation of the dq-axis inductances with the phase angle.

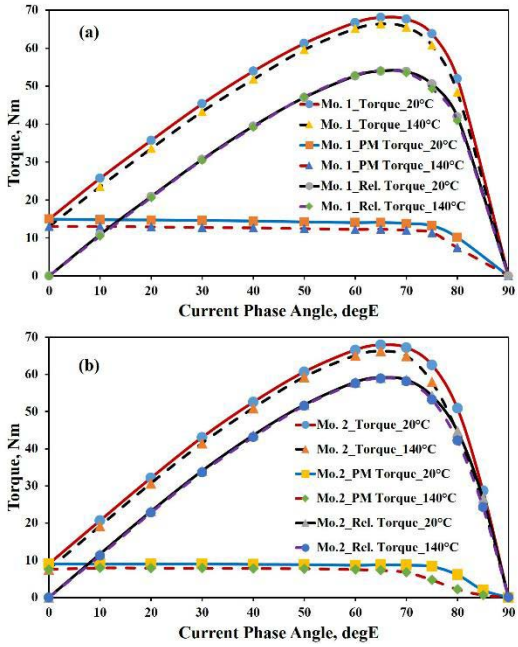

Fig. 7. Torque proportion of PMa-SynRMs with different temperatures. (a) Model 1. (b) Model 2.

flux linkage for both models gradually decay with the current phase angle (an 8.8% drop for Model 1 and 9.8% for Model 2 at 60°E based on that at 0°E). However, the magnitude drops significantly over 65°E (35% at 80°E). This would affect the PM torque proportion in the two models.

As shown in Fig. 6, the d-axis inductance of both models at 80 A excitation current increases slightly for phase angle between 0°E and 60°E and rises significantly from 65°E to 90°E. In contrast, the q-axis inductance maintains with the current phase angle for both models. This indicates that the reluctance torque of both models would significantly increase beyond 65°E.

Then, the torque proportions (i.e., reluctance torque and PM torque) of the two PMa-SynRMs with the influence of temperature are investigated. The performance of the motors in the FW region is considered here, where the demagnetization of PM can easily occur with temperature effect. Fig. 7 shows the torque proportion of the two models with 80 A maximum current and variable current phase angle at the 20 °C and 140 °C magnet temperatures. The maximum torque of the two motors is 67.9 and 68.1 Nm at the 20 °C magnet temperature

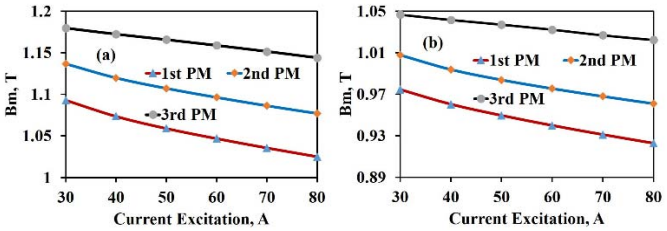

Fig. 8. Effect of the excitation current to the PM flux density of PMs in Model 1 with different temperatures. (a) 20 °C. (b) 140 °C.

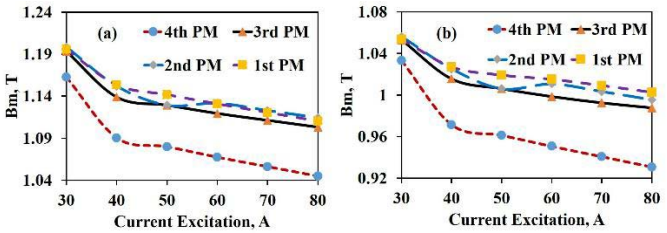

Fig. 9. Effect of the excitation current to the PM flux density of PMs in Model 2 with different temperatures. (a) 20 °C. (b) 140 °C.

with 65°E current phase angle. Also, the PM torque slightly decreases by 8.8% for Model 1 and 9.7% for Model 2 at current phase 60°E (compared to that at 0°E) and significantly reduces beyond 65°E. This matches the analysis for the trend of flux linkage shown in Fig. 5.

When the magnet temperature increases to 140 °C, the total torque reduces about 5% for Model 1 and 7.5% for Model 2. The primary cause for torque reduction is the proportion of PM torque that has significantly decreased, particularly at the phase angle between 65°E and 90°E (e.g., 26.3% PM torque drop for Model 1 and 64.3% for Model 2 compared to that at 20 °C). Meanwhile, the proportion of reluctance torque only slightly reduces with 140 °C magnet temperature, as shown in Fig. 7. This makes the PMa-SynRMs operate as SynRMs when demagnetization of PMs occurs. Therefore, it can be observed that the demagnetization of PMs in PMa-SynRMs can easily occur under the combined effect of the excitation current, its phase angle and high temperature. In particular, the current phase angle may play a key role in demagnetization of the motors. This should be considered and evaluated carefully.

IV. Factors Affecting PM Demagnetization

A. Effect of Excitation Current to PM Demagnetization

Figs. 8 and 9 show the effect of the excitation current at 0°E phase angle on the PM flux density for Models 1 and 2 with different temperatures. It can be seen that the flux density produced in the PMs for both models slightly reduces toward the outward PM positions and also decreases as the current increase from 30 to 80 A at 20 °C. The maximum demagnetization ratio for Model 1 is 6.22% at position 1 although the PM size and flux density at this position are the highest [Fig. 8(a)]. Meanwhile, the maximum demagnetization ratio for Model 2 is 10.14% at position 4 [Fig. 9(a)]. Thus, the PM flux density at position 4 is lower than other positions although the PM size

TABLE III
Effect of Current Excitation to PM Demagnetization at 0°E Phase Advance of Model 1

Items	1st PM	2nd PM	3rd PM
Part 1: At 20^{0}C magnet temperature			
(A) B_m FEA (T) @ 30A	1.093	1.137	1.18
(B) B_m FEA (T) @ 80A	1.025	1.08	1.144
[1-(B)/(A)][%]	6.22%	5.01%	3.05%
Part 2: At 140^{0}C magnet temperature			
(C) B_m FEA (T) @ 30A	0.975	1.01	1.047
(D) B_m FEA (T) @ 80A	0.923	0.961	1.022
[1-(C)/(A)][%]	10.8%	11.1%	11.3%
[1-(D)/(B)][%]	10%	11%	10.7%

TABLE IV
Effect of Current Excitation to PM Demagnetization at 0°E Phase Advance of Model 2

Items	1st PM	2nd PM	3rd PM	4th PM
Part 1: At 20^{0}C magnet temperature				
(A) B_m FEA (T) @ 30A	1.196	1.198	1.193	1.163
(B) B_m FEA (T) @ 80A	1.110	1.114	1.103	1.045
[1-(B)/(A)][%]	7.13%	7.04%	7.56%	10.14%
Part 2: At 140^{0}C magnet temperature				
(C) B_m FEA (T) @ 30A	1.054	1.056	1.053	1.033
(D) B_m FEA (T) @ 80A	1.0	0.996	0.988	0.931
[1-(C)/(A)][%]	11.87%	11.87%	11.75%	11.2%
[1-(D)/(B)][%]	9.7%	10.66%	10.46%	10.9%

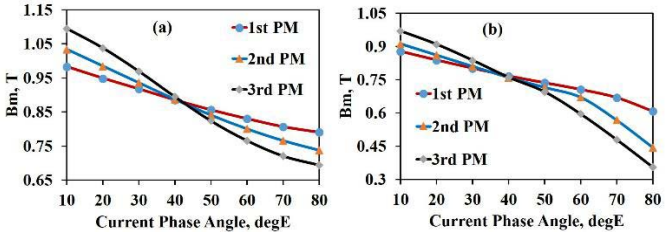

Fig. 10. Effect of the current phase angle to the PM flux density of Model 1 with different temperatures. (a) 20 °C. (b) 140 °C.

is the same for all positions in Model 2. When the magnet temperature increases to 140 °C, the demagnetization ratio of PMs varies from 9.7% to 11.8% for both models although they can occur at PM different positions [Figs. 8(b) and 9(b)]. In addition, the increase in the excitation current leads to the increase in the motor temperature, but it does not significantly affect the demagnetization of PMs in the PMa-SynRM. The effect of the excitation current to PM demagnetization for the two models is summarized and shown in Tables III and IV.

B. Effect of Current Phase Angle to PM Demagnetization

Figs. 10 and 11 show the effect of the current phase angle at 80 A peak current excitation to the PM flux density for Models 1 and 2, respectively, with different temperatures. As can be seen, the flux density at each PM position for the two models is different and the demagnetization ratio of PMs under the effect of the current phase angle considering temperature

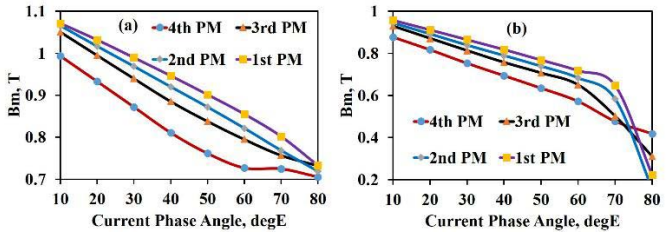

Fig. 11. Effect of the current phase angle to the PM flux density of Model 2 with different temperatures. (a) 20 °C. (b) 140 °C.

TABLE V
EFFECT OF THE CURRENT PHASE ANGLE TO PM DEMAGNETIZATION AT 80 A CURRENT EXCITATION OF MODEL 1

Items	1st PM	2nd PM	3rd PM
Part 1: At 20^{0}C magnet temperature			
(A) B_m FEA (T) @ 10^{0}E	0.983	1.034	1.095
(B) B_m FEA (T) @ 80^{0}E	0.79	0.738	0.694
[1-(B)/(A)][%]	19.6%	28.6%	36.6%
Part 2: At 140^{0}C magnet temperature			
(C) B_m FEA (T) @ 10^{0}E	0.879	0.913	0.97
(D) B_m FEA (T) @ 80^{0}E	0.608	0.444	0.355
[1-(C)/(A)][%]	10.6%	11.7%	11.4%
[1-(D)/(B)][%]	23.1%	39.8%	48.9%

is also different. When the current phase angle increases from 10°E to 80°E at 20 °C, the demagnetization ratio is significantly affected. The maximum demagnetization ratio is about 36.6% at position 3 for Model 1 and 32.6% at position 2 for Model 2, respectively, as shown in Figs. 10(a) and 11(a). When the magnet temperature is 140 °C, the PM flux density of the two models reduces significantly, with a dependence on PM position, as shown in Figs. 10(b) and 11(b). This would result in irreversible demagnetization for both PMa-SynRMs with the demagnetization ratio being 48.9% at position 3 for Model 1 and 69.7%, 78.3%, and 57.5% at positions 1, 2, and 3 for Model 2. This shows that the main reason for irreversible demagnetization is the current phase angle combining high temperature. Moreover, the irreversible demagnetization of PMs can also be caused significantly by position and size in the rotor core of the PMa-SynRM. The effect of the current phase angle to PM demagnetization for the two models is summarized and shown in Tables V and VI.

C. Results of the Demagnetization in PMs of PMa-SynRM

As previously mentioned, the irreversible demagnetization occurred in multilayer magnets of the PMa-SynRM by the effect of the current phase angle combining temperature effect. Based on the motor performance required over a wide speed range and the effect of current excitation, current phase angle, and magnet temperature, the irreversible demagnetization can be found to occur at 2500 rpm, 80 A peak current, 80°E current phase angle, and 135 °C magnet temperature for Model 1 [Fig. 12(a)]. For Model 2, this occurs at 3000 rpm, 80 A peak current excitation, 84°E current phase angle, and 130 °C magnet temperature [Fig. 12(b)]. These demagnetization points

TABLE VI
EFFECT OF THE CURRENT PHASE ANGLE TO PM DEMAGNETIZATION AT 80 A CURRENT EXCITATION OF MODEL 2

Items	1st PM	2nd PM	3rd PM	4th PM
Part 1: At 20^{0}C magnet temperature				
(A) B_m FEA (T) @ 10^{0}E	1.072	1.066	1.05	0.993
(B) B_m FEA (T) @ 80^{0}E	0.733	0.719	0.732	0.705
[1-(B)/(A)][%]	31.6%	32.6%	30.3%	29%
Part 2: At 140^{0}C magnet temperature				
(C) B_m FEA (T) @ 10^{0}E	0.958	0.944	0.929	0.878
(D) B_m FEA (T) @ 80^{0}E	0.222	0.156	0.311	0.417
[1-(C)/(A)][%]	10.6%	11.4%	11.5%	11.6%
[1-(D)/(B)][%]	69.7%	78.3%	57.5%	40.9%

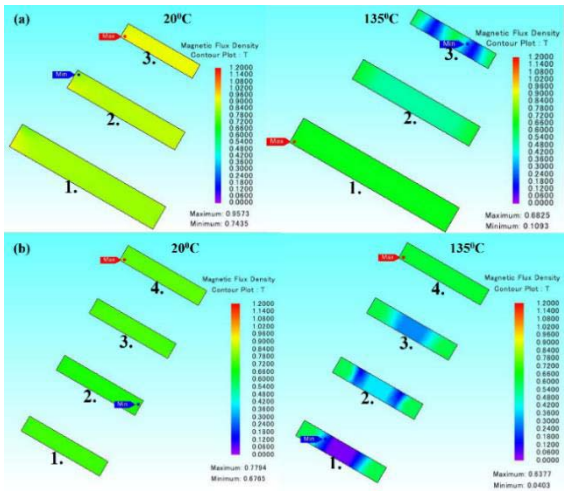

Fig. 12. PM flux density distribution at each position of two PMa-SynRMs at 20 °C and 135 °C. (a) Model 1. (b) Model 2.

fall within the FW region where the demagnetization can be easier than other regions for PMa-SynRMs. In addition, the maximum demagnetization ratio mostly appears to be close to the center of the PMs at position 3 for the Model 1 and positions 1, 2, and 3 for Model 2. This might be attributed to a higher temperature distribution at the center of the PMs than at the edges under strong armature field [10], [11]. Therefore, the operating point of PMs at these positions is further pushed down. The overall results of demagnetization in PMs for the two PMa-SynRMs are shown in Fig. 13 and Table VII.

D. Discussion

With the above analysis results, the demagnetization problem for the PMa-SynRM can be summarized as follows.

1) The operating condition of a motor significantly affects the demagnetization possibility of PM, especially in the FW region.
2) The design of Model 2 is more vulnerable to demagnetization than that of Model 1 since the PM size is too small to resist demagnetization.
3) The distribution of the magnetic flux density at each PM position in PMa-SynRMs is significantly affected by the current phase angle, particularly at high-temperature operation.

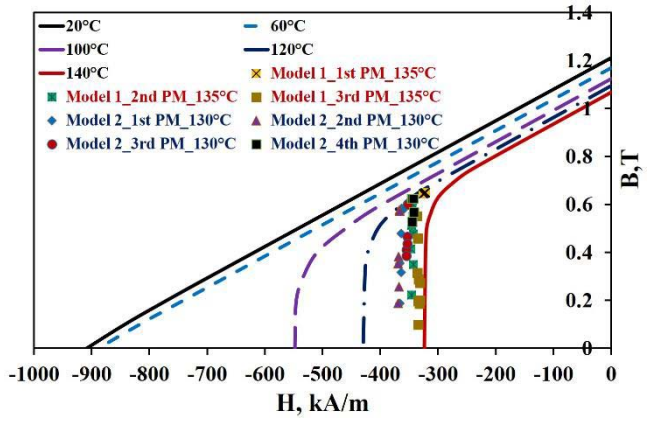

Fig. 13. Demagnetization curves and operating points of the PM in Models 1 and 2 considering the temperature effect.

TABLE VII
PM FLUX DENSITY WITH THE INCREASING TEMPERATURE AT LOAD CONDITION

Items	1st PM	2nd PM	3rd PM	4th PM
Part 1: At 80A, 80^{0}E phase angle of Model 1				
(A) B_m FEA (T) @ 20^{0}C	0.79	0.738	0.694	-
(B) B_m FEA (T) @ 135^{0}C	0.646	0.512	0.285	-
[1-(B)/(A)][%]	18.3%	30.6%	58.9%	-
Part 2: At 80A, 84^{0}E phase angle of Model 2				
(A) B_m FEA (T) @ 20^{0}C	0.713	0.705	0.73	0.742
(B) B_m FEA (T) @ 130^{0}C	0.246	0.3	0.391	0.594
[1-(B)/(A)][%]	65.4%	57.9%	46.5%	20%

V. DESIGN METHOD TO AVOID THE DEMAGNETIZATION

A. Proposed Design Method

Based on the analysis results, Model 2 is selected for further study and the PM sizes in the rotor core will be redesigned to avoid demagnetization. To do this, the calculation to compensate for the lost flux quantity due to temperature should be conducted. A method to calculate the new PM sizes is proposed, as shown in Fig. 14, which is explained in the following.

1) The index "demagnetization ratio" is first calculated for each PM. The demagnetization ratio due to temperature and operating conditions (FW region) at positions 1, 2, 3, and 4 is 65.4%, 57.9%, 46.5%, and 20%, respectively. However, the irreversible demagnetization only occurred for the PM at positions 1, 2, and 3. Thus, the PM flux density at position 4 is utilized as the minimum flux density base which the other PM positions should achieve after the redesign.
2) The new operating points of the PMs are calculated by the nonlinear analysis, applying the convergence method considering temperature and operation conditions, as can be found in [18].
3) To avoid demagnetization for the PM at position 4 after the redesign, the width of the four PM layers for Model 2 is maintained but the thickness of these PMs would be adjusted. Then, the equivalent magnetic circuit that was developed in [4], [5], and [19] is applied to the calculation of the PM thickness based on the new operating points.

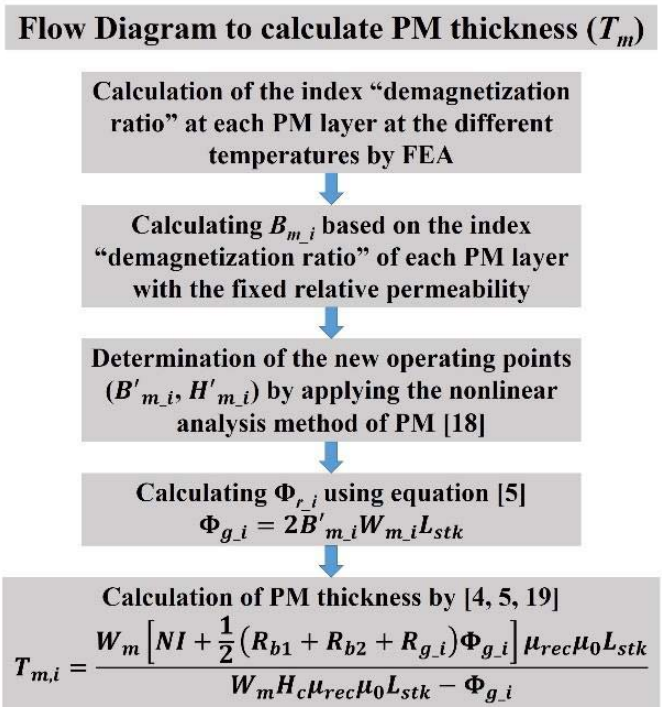

Fig. 14. Flowchart to calculate new PM volume of the PM-SynRM.

TABLE VIII
COMPARISON OF THE PM FLUX DENSITY WITH DIFFERENT TEMPERATURES AFTER REDESIGN

Items	1st PM	2nd PM	3rd PM	4th PM
PM size (mm)	2 x 8	1.8 x 8	1.7 x 8	1.5 x 8
(A) B_m FEA (T) @ 20^{0}C after	0.828	0.79	0.785	0.746
(B) B_m FEA (T) @ 20^{0}C before	0.713	0.705	0.73	0.742
[1-(B)/(A)][%]	13.9%	10.8%	7%	0.54%
(C) B_m Calculation (T) @ 130^{0}C	0.729	0.691	0.689	0.66
(D) B_m FEA (T) @ 130^{0}C after	0.693	0.654	0.645	0.610
(E) B_m FEA (T) @ 130^{0}C before	0.246	0.3	0.362	0.556
[1-(D)/(C)][%]	4.67%	3.54%	3.41%	7.6%
[1-(E)/(D)][%]	64.5%	54.1%	43.9%	8.8%

B. Results

Based on the proposed design method, the new PM sizes at positions 1, 2, and 3 are calculated and redesigned while the PM size at position 4 is maintained. Then, the FEA is applied to validate the performance and demagnetization of the PMa-SynRM with the new PM sizes. The analysis result shows that the operating point of the PMs at positions 1, 2, and 3 without load condition increases by about 13.9%, 10.8%, and 7%, respectively, after employing new PMs. In the load condition, the flux density of the PMs at positions 1, 2, and 3 also increases by about 64.5%, 54.1%, and 43.9%, respectively. The operating points of the old and new PMs are compared and shown in Table VIII. The simulated PM flux density at each position for the redesign is slightly

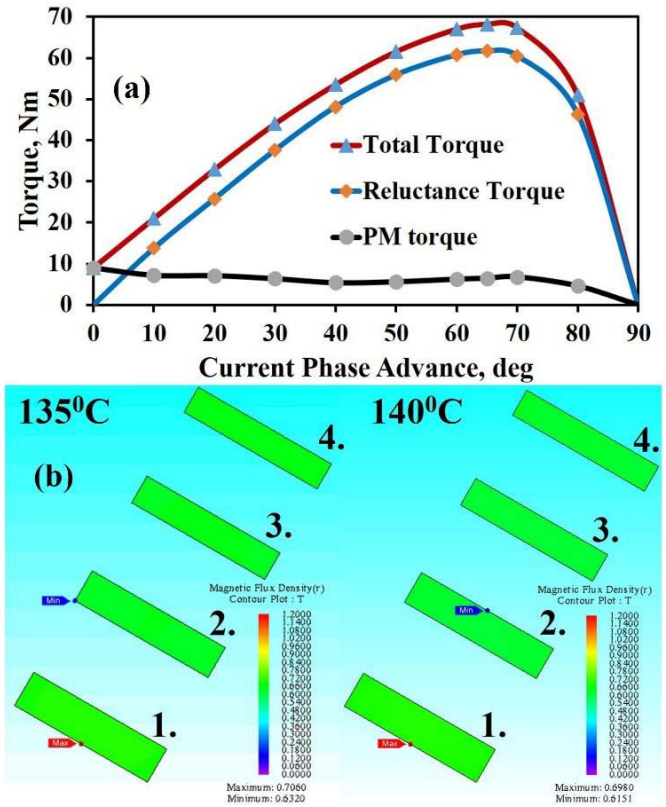

Fig. 15. (a) Total torque, PM torque, and reluctance torque. (b) Flux density distribution at each PM position after recalculation of PM sizes for different positions at 135 °C and 140 °C.

Fig. 16. Prototype of the PMa-SynRM without magnets.

different from the calculation. This is possible because the effect of eddy current in the magnets was not considered in the simulation. Fig. 15 shows the motor torque and flux density distribution at each PM position. As can be seen, the demagnetization problem has been resolved with the new PM sizes for the magnet temperature achieving 140 °C. The motor torque achieves 68 Nm that is slightly higher than the original motor.

VI. Measurements

A prototype PMa-SynRM was fabricated based on Model 2, as shown in Fig. 16. The comparison of the magnetic flux density on the rotor surface (without the stator) between the simulation and measurement is shown in Fig. 17, where the two cases agree well. Therefore, the simulation results should be sufficiently reliable. The measurement for the

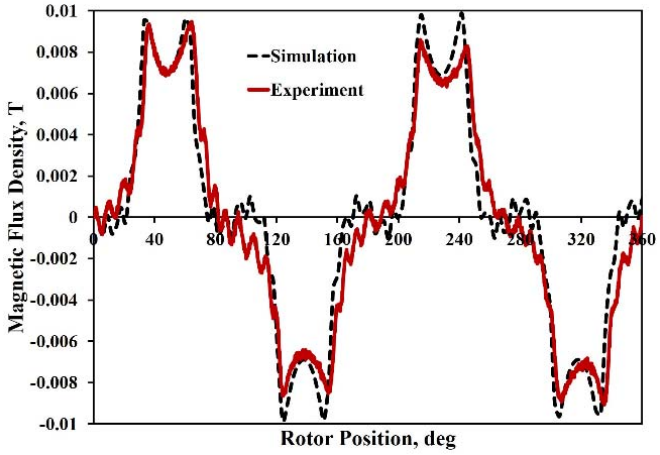

Fig. 17. Comparison of the flux density on the rotor surface of the PMa-SynRM between simulation and measurement.

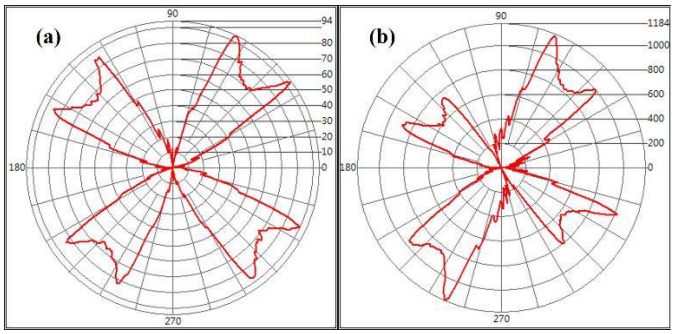

Fig. 18. Comparison of flux density on the rotor of the PMa-SynRM for normal and demagnetized conditions. (a) Undemagnetized. (b) Demagnetized. The values are the resolution of the measurements.

demagnetization condition is shown in Fig. 18. The demagnetization measurement is implemented on the rotor surface with the rotor taken out of the motor after an 80 A, 65°E current was applied. The comparison before and after the demagnetization test shows that the flux density distribution distorts in the demagnetized case, as indicated in Fig. 18(b). Note that the flux density distribution on rotor was tested at different times and resolutions for different projects so the measured ranges are different for Fig. 18(a) and (b). Overall, the test results validate the analysis method. Note that the open circuit measurements and the tests with load were partly reported in [20], where the simulation was validated.

VII. Conclusion

This paper has investigated the demagnetization in multilayer magnets for two PMa-SynRMs. The investigation has found that the current phase angle combining high temperature would most significantly affect the demagnetization in the multilayer magnets. Demagnetization also depends on the position and volume of PM in the rotor of the PMa-SynRM. The center of one PM piece is more easily demagnetized than the edges due to higher temperature and flux density. Then, the method has been proposed such that the

PM volume can be redesigned to compensate for the lost flux density quantity in the initial design stage and avoid demagnetization. The analysis result has been validated by the experiments.

ACKNOWLEDGMENT

This work was supported by Ministry of Science and Technology, Taiwan, under Projects MOST 107-2622-8-006-015 and MOST 107-2221-E-006-211. The assistance of the members in Electrical Machine and Drive System Laboratory during experiments is highly appreciated. The author would like to thank JSOL for supporting JMAG software.

REFERENCES

[1] R. Cao, C. Mi, and M. Cheng, "Quantitative comparison of flux-switching permanent-magnet motors with interior permanent magnet motor for EV, HEV, and PHEV applications," *IEEE Trans. Magn.*, vol. 48, no. 8, pp. 2374–2384, Aug. 2012.

[2] P. Guglielmi, B. Boazzo, E. Armando, G. Pellegrino, and A. Vagati, "Permanent-magnet minimization in PM-assisted synchronous reluctance motors for wide speed range," *IEEE Trans. Ind. Appl.*, vol. 49, no. 1, pp. 31–41, Jan./Feb. 2013.

[3] T. A. Huynh and M.-F. Hsieh, "Comparative study of PM-assisted SynRM and IPMSM on constant power speed range for EV applications," *IEEE Trans. Magn.*, vol. 53, no. 11, Nov. 2017, Art. no. 8211006.

[4] K.-C. Kim, K. Kim, H. J. Kim, and J. Lee, "Demagnetization analysis of permanent magnets according to rotor types of interior permanent magnet synchronous motor," *IEEE Trans. Magn.*, vol. 45, no. 6, pp. 2799–2802, Jun. 2017.

[5] T. A. Huynh, M.-F. Hsieh, K.-J. Shih, and H.-F. Kuo, "An investigation into the effect of PM arrangements on PMa-SynRM performance," *IEEE Trans. Ind. Appl.*, vol. 54, no. 6, pp. 5856–5868, Nov./Dec. 2018.

[6] P. Zhou, D. Lin, Y. Xiao, N. Lambert, and M. A. Rahman, "Temperature-dependent demagnetization model of permanent magnets for finite element analysis," *IEEE Trans. Magn.*, vol. 48, no. 2, pp. 1031–1034, Feb. 2012.

[7] S. Ruoho, J. Kolehmainen, J. Ikaheimo, and A. Arkkio, "Interdependence of demagnetization, loading, and temperature rise in a permanent-magnet synchronous motor," *IEEE Trans. Magn.*, vol. 46, no. 3, pp. 949–953, Mar. 2010.

[8] D. D. Reigosa, D. Fernandez, T. Tanimoto, T. Kato, and F. Briz, "Permanent-magnet temperature distribution estimation in permanent-magnet synchronous machines using back electromotive force harmonics," *IEEE Trans. Ind. Appl.*, vol. 52, no. 4, pp. 3093–3103, Jul./Aug. 2016.

[9] D. D. Reigosa, D. Fernandez, H. Yoshida, T. Kato, and F. Briz, "Permanent-magnet temperature estimation in PMSMs using pulsating high-frequency current injection," *IEEE Trans. Ind. Appl.*, vol. 51, no. 4, pp. 3159–3168, Jul./Aug. 2015.

[10] A. M. El-Refaie, N. C. Harris, T. M. Jahns, and K. M. Rahman, "Thermal analysis of multibarrier interior PM synchronous machine using lumped parameter model," *IEEE Trans. Energy Convers.*, vol. 19, no. 2, pp. 303–309, Jun. 2004.

[11] X. Ding, J. Liu, and C. Mi, "Online temperature estimation of IPMSM permanent magnets in hybrid electric vehicles," in *Proc. 6th IEEE Conf. Ind. Electron. Appl.*, Beijing, China, Jun. 2011, pp. 179–183.

[12] S. Ohta. (Dec. 1985). *Temperature Classes of Electrical Insulators*. [Online]. Available: http://www.threebond.co.uk/Portals/0/tech13

[13] V. Ghorbanian, S. Hussain, S. Hamidizadeh, R. Chromik, and D. Lowther, "The role of temperature-dependent material properties in optimizing the design of permanent magnet motors," *IEEE Trans. Magn.*, vol. 54, no. 3, Mar. 2018, Art. no. 8101104.

[14] Eclipse Magnetics Ltd, *Sintered Neodymium Iron Boron (NdFeB) Magnets*. Accessed: Apr. 2019. [online]. Available: https://www.eclipse-magnetics.com/media/wysiwyg/brochures/neodymium_grades_data.pdf

[15] M. H. A. Prins, "Design of a field-intensified interior permanent magnet synchronous machine for electric vehicle application," M.S. thesis, Elect. Electron. Eng., Univ. Stellenbosch, Stellenbosch, South Africa, Mar. 2014.

[16] H. Huang, Y.-S. Hu, Y. Xiao, and H. Lyu, "Research of parameters and antidemagnetization of rare-earth-less permanent magnet-assisted synchronous reluctance motor," *IEEE Trans. Magn.*, vol. 51, no. 11, Nov. 2015, Art. no. 8112504.

[17] H.-K. Kim and J. Hur, "Dynamic characteristic analysis of irreversible demagnetization in SPM-and IPM-type BLDC motors," *IEEE Trans. Ind. Appl.*, vol. 53, no. 2, pp. 982–990, Mar./Apr. 2017.

[18] M.-R. Park, H.-J. Kim, Y.-Y. Choi, J.-P. Hong, and J.-J. Lee, "Characteristics of IPMSM according to rotor design considering nonlinearity of permanent magnet," *IEEE Trans. Magn.*, vol. 52, no. 3, Mar. 2016, Art. no. 8101904.

[19] W.-H. Kim *et al.*, "Optimal PM design of PMA-SynRM for wide constant-power operation and torque ripple reduction," *IEEE Trans. Magn.*, vol. 45, no. 10, pp. 4660–4663, Oct. 2009.

[20] T. A. Huynh and M.-F. Hsieh, "Performance analysis of permanent magnet motors for electric vehicles (EV) traction considering driving cycles," *Energies*, vol. 11, no. 6, p. 1385, Jun. 2018.